

Managing Axle Saturation for Vehicle Stability Control with Independent Wheel Drives

Justin H. Sill and Beshah Ayalew, *Member, ASME, IEEE*

Abstract— This paper proposes a new stability control method that quantifies and uses the level of lateral force saturation on each axle of a vehicle featuring an independent wheel drive system. The magnitude of the saturation, which can be interpreted as a slip-angle deficiency, is determined from estimated nonlinear axle lateral forces and comparisons with linear projections that use estimates of the cornering stiffness. Once known, the per-axle saturation levels are employed in a saturation balancing control structure that biases the drive/brake torque to either the front or rear axles with the goal of minimizing excessive under- or over-steer. The approach is then combined with a direct yaw-moment controller to obtain enhanced stability and responsiveness. The benefits of the proposed approach are demonstrated for a nominally unstable vehicle in an extreme obstacle avoidance type maneuver.

I. INTRODUCTION

Vehicle stability control (VSC) systems help reduce accidents by minimizing driver's loss of control of the vehicle during emergency/aggressive maneuvers. Most VSC (also referred to as vehicle dynamics control (VDC)) systems available on the market today are brake-based which mainly extend the functionality of mature hardware technology available for anti-lock braking systems. They facilitate differential (left-to-right) braking to generate the required corrective or stabilizing yaw moment [1-4]. However, this strategy slows the vehicle against driver intent, leading to wasted energy through heat and contributing to accelerated wear of the friction brakes. An alternative approach for generating the corrective yaw moment that avoids the drawbacks of brake-based strategies is to distribute the tractive/braking force differentially between driving wheels [5-8]. Current solutions based on this strategy include the so-called torque-vectoring systems which employ active differentials within conventional power trains [9, 10].

In this paper, the focus is on outlining a new stability control method suitable for vehicles with independent drive systems that act on each wheel (or axle) of the vehicle. Such drive systems can be configured in series electric hybrids, pure electric, fuel cell powered and hydraulic hybrid vehicles. These systems allow stability control functions wherein the traction/braking force of each wheel is

manipulated via the torque output of the individual wheel drive units (motors).

For vehicles with independent drive systems, several direct yaw-moment controllers (yaw rate feedback, lateral acceleration feedback or combined feedback), and torque distribution strategies have been previously assessed for some strengths and weaknesses in [7, 11]. These approaches are rather simplistic in that the stabilizing yaw moments were distributed to the individual wheels largely based on pre-determined rules. In this paper, a method is outlined for biasing the front-to-rear torque distribution based on online estimation of the level of saturation on each axle. A feedback controller is setup to reduce the imbalance in the level of saturation between the front and rear axles and thereby stabilize the vehicle. For enhanced performance, this controller can also be combined with a direct yaw-moment controller that solely distributes torque side-to-side.

The rest of this paper is organized as follows. The requisite system modeling is briefly outlined in Section II. Section III outlines the vehicle stability control and details the proposed method. Section V presents demonstrative results for an aggressive maneuver considering an otherwise unstable vehicle. Finally, section VI presents the conclusions of the work.

II. SYSTEM MODELING

A 7-DOF model is used to represent the handling dynamics for performance evaluations of the developed control strategies. The model includes the degrees of freedom of lateral and longitudinal motions, yaw rotation, and the rotations of the four tires. This model ignores suspension effects and therefore does not consider the pitch, heave, and roll of the vehicle body. Detailed derivations and discussions of the model are given in [7, 8, 12]. The longitudinal, lateral, and yaw equations of motion are:

$$\begin{aligned}
 m(\dot{V}_x - V_y \dot{\psi}) &= \sum F_x \\
 &= (F_{xLF} + F_{xRF}) \cos(\delta) - (F_{yLF} + F_{yRF}) \sin(\delta) \\
 &\quad + F_{xLR} + F_{xRR} - \frac{1}{2} \rho C_D A V_x^2 - mg C_{rr}
 \end{aligned} \tag{1}$$

$$\begin{aligned}
 m(\dot{V}_y + V_x \dot{\psi}) &= \sum F_y \\
 &= (F_{yLF} + F_{yRF}) \cos(\delta) + (F_{xLF} + F_{xRF}) \sin(\delta) \\
 &\quad + F_{yLR} + F_{yRR}
 \end{aligned} \tag{2}$$

Final manuscript received April 6, 2010.

J. Sill is with Clemson University International Center for Automotive Research, Greenville, SC 29607, USA (e-mail: jsill@clemson.edu).

B. Ayalew is with Clemson University International Center for Automotive Research, Greenville, SC 29607, USA (Corresponding author: phone: 864-283-7228; e-mail: beshah@clemson.edu).

$$\begin{aligned}
I_{zz}\ddot{\psi} &= \sum M_z \\
&= l_f [(F_{yLF} + F_{yRF})\cos(\delta) + (F_{xLF} + F_{xRF})\sin(\delta)] \\
&\quad + \frac{d_f}{2} [(F_{xRF} + F_{xLF})\cos(\delta) + (F_{yLF} - F_{yRF})\sin(\delta)] \quad (3) \\
&\quad + l_r (F_{yLR} + F_{yRR}) + \frac{d_r}{2} (F_{xRR} - F_{xLR})
\end{aligned}$$

The notations used in (1-3) are defined in Figure 1.

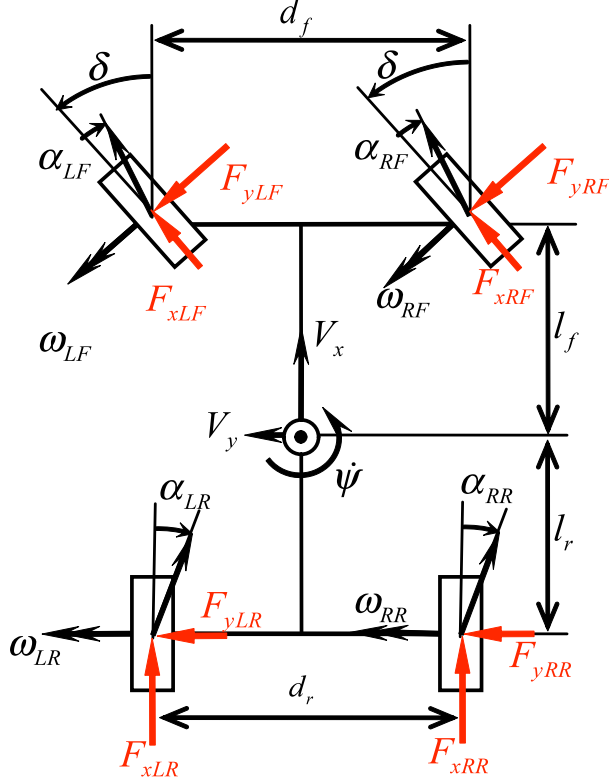


Fig. 1. Schematic of Vehicle Dynamics Model

The tire/wheel dynamics connect the wheel torque to the dynamics of the vehicle via the longitudinal tire forces. The tire/wheel dynamics are given by:

$$I_w \dot{\omega}_i = T_{w,i} - F_{x,i} R_w \quad (4)$$

where i represents left front, right front, left rear, and right rear tires.

Each wheel torque is determined from a vehicle speed controller (or driver model) and/or the vehicle stability controller described in the next section. Ideally, the wheel torques, T_w , will be achieved through driving and primarily regenerative braking, however, friction-based braking will be used as a supplement when regenerative braking alone cannot give the desired level of deceleration.

The tire forces are determined by the operating conditions for each tire, specifically, normal loads, longitudinal slip ratios, and lateral slip angles. Considering the load transfers that occur due to lateral and longitudinal accelerations and differences in the front and rear roll-stiffness distributions, the prevailing tire normal loads can be computed within the simplified 7 DOF model described above. The loads for the left front and left rear tires are given by (others follow similarly):

$$\begin{aligned}
F_{zLF} &= \frac{mgl_r}{2L} - A_x \left(\frac{mh_{cg}}{2L} \right) \\
&\quad - A_y \left(\frac{ml_r h_{rcF}}{Ld_f} + \frac{m(h_{cg} - h_{rcF})\kappa_{\phi F}}{d_f (\kappa_{\phi F} + \kappa_{\phi R} - mg(h_{cg} - h_{rcF}))} \right) \\
F_{zLR} &= \frac{mgl_f}{2L} + A_x \left(\frac{mh_{cg}}{2L} \right) \\
&\quad - A_y \left(\frac{ml_f h_{rcR}}{Ld_r} + \frac{m(h_{cg} - h_{rcR})\kappa_{\phi R}}{d_r (\kappa_{\phi F} + \kappa_{\phi R} - mg(h_{cg} - h_{rcR}))} \right) \quad (5)
\end{aligned}$$

The tire slip ratios and slip angles are computed from the vehicle's longitudinal and lateral velocities, yaw rate, wheel spin and steer angle as (others follow similarly):

$$\kappa_i = \frac{\omega_i R_w}{V_{xi}} - 1 \quad (6)$$

$$\alpha_{LF} = \tan^{-1} \left(\frac{V_y + l_f \dot{\psi}}{V_x + \frac{d_f}{2} \dot{\psi}} \right) - \delta \quad \text{and} \quad \alpha_{LR} = \tan^{-1} \left(\frac{V_y - l_f \dot{\psi}}{V_x + \frac{d_f}{2} \dot{\psi}} \right) \quad (7)$$

Since longitudinal tractive forces of each wheel are to be exploited to influence the lateral handling dynamics, a proper tire model that considers combined slip conditions (longitudinal and lateral) must be used, i.e. models that give $F_x = F_x(\kappa, \alpha, F_z)$ and $F_y = F_y(\kappa, \alpha, F_z)$ are needed. In combined slip conditions, when the longitudinal slip ratio approaches its extreme values ($\kappa = -1$ or ∞) there is no lateral force capacity. Conversely, when the lateral slip angle α becomes extreme, the longitudinal force capacity reduces to small values. In the present work, combined slip tire data provided in [13] are suitably scaled and implemented as a multi-dimensional lookup table.

III. STABILITY CONTROL METHOD

The following sections outline the development of the vehicle control strategies. Section A proposes the definition and calculation of axle saturation. Section B and C presents a basic front-rear torque biasing control using the calculated axle saturations as well as a direct yaw moment control through right-left torque variations. Finally, Section D discusses the cascading implementation of these strategies.

A. Estimation of Axle Saturation

To achieve vehicle stability, the net torque may be divided between the front and rear axles in such a way as to balance axle lateral force capacity. In order to accomplish, a method is needed to determine the axle lateral force capacity and therefore the level of axle saturation from available vehicle dynamics sensors. This can be accomplished by estimating the lateral tire forces and estimating axle slip angles.

The front and rear lateral forces can be determined by the inverse of a two degree of freedom handling model given the measured lateral acceleration, yaw rate, steering angle, and estimated longitudinal tire forces. This approach has been derived in previous papers [2, 14] and defines the axle forces as:

$$\begin{Bmatrix} F_{yF,est} \\ F_{yR,est} \end{Bmatrix} = \begin{bmatrix} \cos \delta & \cos \delta \\ a & -b \end{bmatrix}^{-1} \left\{ \begin{bmatrix} mA_y \\ I_{zz} \frac{d\dot{\psi}}{dt} \end{bmatrix} - M_x \right\} \quad (8)$$

where,

$$M_x = \begin{bmatrix} \sin \delta & \sin \delta & 0 & 0 \\ a \sin \delta - \frac{d_f}{2} \cos \delta & a \sin \delta + \frac{d_f}{2} \cos \delta & -\frac{d_r}{2} & \frac{d_r}{2} \end{bmatrix} \begin{bmatrix} F_{xLF,est} \\ F_{xRF,est} \\ F_{xLR,est} \\ F_{xRR,est} \end{bmatrix}$$

Longitudinal tire forces that are corrected for wheel rotational inertia can be estimated from the controlled torque and speed sensors for each wheel as [2, 4]:

$$F_{xi,est} = T_i - I_w \frac{d\omega_i}{dt} \quad (9)$$

To demonstrate the main idea proposed in this paper, the axle slip angles are determined from the lateral velocity estimate which is simply obtained from the sensor measurements of lateral acceleration, longitudinal velocity, and yaw rate:

$$V_{y,est} = \int (A_y - \dot{\psi} V_x) dt \quad (10)$$

Then the slip angles can be defined by:

$$\alpha_{F,est} = \tan^{-1} \left(\frac{V_{y,est} + a\dot{\psi}}{V_x} \right) - \delta \quad (11)$$

$$\alpha_{R,est} = \tan^{-1} \left(\frac{V_{y,est} - b\dot{\psi}}{V_x} \right) \quad (12)$$

Knowing the axle lateral forces and slip angles for each time instant, the saturation of the axle, C_{sat} , can be determined as the deviation from an expected linear response (cornering stiffness) as shown in Figure 3.

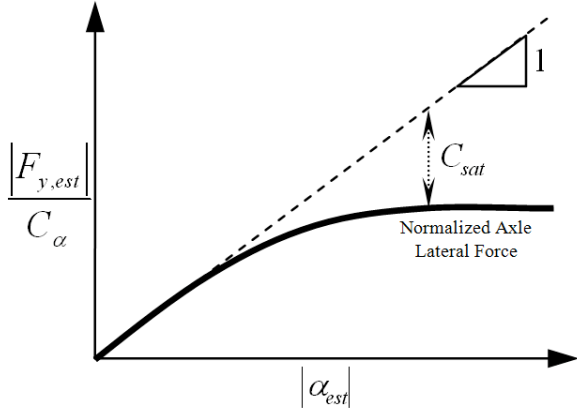


Fig. 2. Axle Force Saturation

Assuming that the axle cornering stiffness is a constant, the axle saturation is defined by:

$$C_{sat} = \frac{F_{y,est}}{C_{\alpha}} - \alpha_{est} \quad (13)$$

The axle saturation defined by (13) can be interpreted as a slip angle deficiency for that axle. It is important to note that the saturation of the front and rear axles occur at different rates and magnitudes. For example, when the front axle saturation is larger than the rear axle saturation ($C_{satF} > C_{satR}$)

the vehicle is experiencing understeer. This situation is depicted in Figure 3. Conversely, an oversteering vehicle can be observed as the rear axle saturates more than the front ($C_{satF} < C_{satR}$).

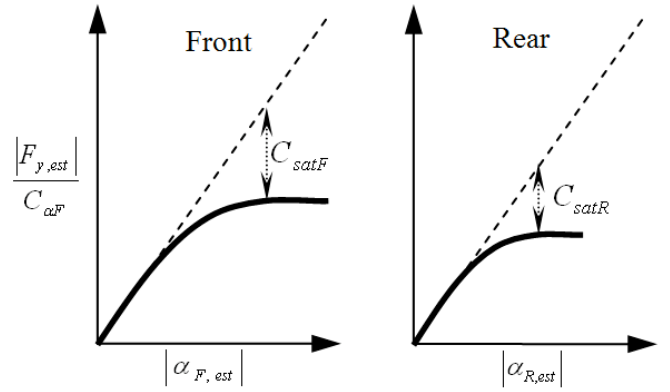


Fig. 3. Axle Force Saturation for Under Steering Vehicle

Ideally, equal levels of saturation for the front and rear axles avoids excessive under or over-steer for the vehicle. This suggests the possibility of using the estimated axle saturation level for feedback control as detailed below.

B. Saturation Balancing Control

It is widely known that the application of a tractive/braking force on front wheel or rear wheel of a vehicle promotes understeer or oversteer in that vehicle, respectively. Therefore, with this in mind a torque biasing PI control is set up using the front and rear axle saturations as follows:

$$\lambda = \left(K_p + \frac{K_I}{s} \right) (C_{satF} - C_{satR}) + \lambda_0 \quad (14)$$

Here, λ is the percent of net torque to the front axle (limited within the range of 0 and 100%) and λ_0 is the initial torque bias for which no control is required. The front and rear axle torque are then given by:

$$T_F = \begin{cases} T_{total} & \lambda > 1 \\ T_{total} \times \lambda & 0 < \lambda < 1 \\ 0 & \lambda < 0 \end{cases} \quad (15)$$

$$T_r = \begin{cases} T_{total} & \lambda < 0 \\ T_{total} \times (1 - \lambda) & 0 < \lambda < 1 \\ 0 & \lambda > 1 \end{cases} \quad (16)$$

C. Combining with Direct Yaw-Moment Control

A direct yaw-moment feedback stability controller (as in [1, 3, 7, 15, 16]) (of a PID type) which compares the desired yaw rate to the actual yaw rate of the vehicle to determine if the vehicle has excessive or insufficient yaw rate (over-steer or under-steer). If excessive yaw rate error is observed, the stability controller acts to reduce the yaw rate error by applying a corrective yaw moment defined by:

$$M_{\psi} = \left(K_p + \frac{K_I}{s} + K_D s \right) (\dot{\psi}_{desired} - \dot{\psi}) \quad (17)$$

where, commonly, $\psi_{\text{desired}} = \frac{V_x \delta}{L + (K_{us} V_x^2)/g}$, i.e., the

steady state yaw rate response to a steering angle input at the given forward velocity. In this scheme, the yaw moment control is achieved through differential torque variations from the left to the right wheels on the axle with the most lateral force capability as determined by λ from above.

D. Overall Vehicle Stability Control Structure

An overall vehicle stability control structure incorporating the above two strategies of axle saturation balancing and direct yaw-moment control is depicted in Figure 4 below.

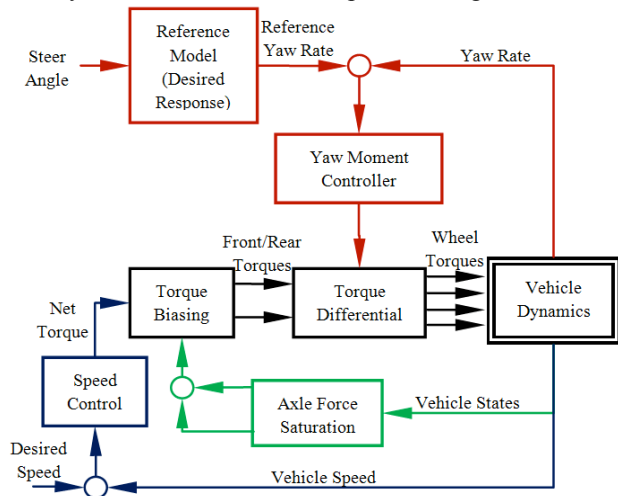


Fig. 4. Schematic of Stability Control Architecture

In the combined scheme, the speed of the vehicle is controlled using a PI controller that computes the base torque required to maintain a desired forward speed. The net torque from the speed controller serves to overcome resistance loads of aerodynamic drag, rolling resistance, and grade. Stability is achieved through the saturation balancing control, which acts to limit excessive under- or over-steer of the vehicle. Finally, the direct yaw-moment control component can be tuned to maintain responsiveness of the vehicle by directing the torques on the left and right wheels of the dominant axle that has the better grip, i.e, the one with the lower level of saturation as identified from the axle force/saturation level estimation.

IV. RESULTS

The above stability control methods were applied to a medium duty truck with a GVW of 8000 lbs and with an upgraded power train featuring independent wheel drives. The vehicle considered is a nominally over-steering vehicle (a worst-case scenario) with front-rear distributions of 55%-45% in weight, 40%-60% in initial drive and 40%-60% in roll stiffness, and on dry asphalt road ($\mu=1.0$). The control gains selected maximize the effectiveness of each control strategy, for comparisons of best-performing responses.

To evaluate the handling performance in aggressive maneuvers, a “sine with dwell” steering angle input was considered. This open-loop maneuver has been defined by NHTSA in the US to emulate a severe obstacle avoidance

type maneuver for evaluating VSC systems by inducing a dynamic nonlinear vehicle response [17]. The uncontrolled, saturation balancing controlled, and combined stability controlled (saturation balancing and direct yaw-moment control) vehicle responses are shown in Figure 5 for this maneuver at 100 kph.

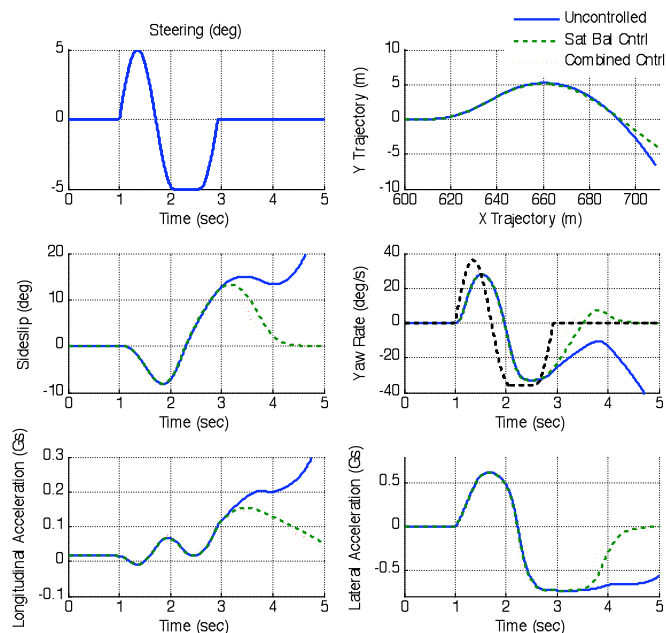


Fig. 5. “Sine with Dwell” Vehicle Response for Uncontrolled & Controlled (saturation balancing and combined control) Power Trains

It can be seen from the figure that the uncontrolled response of the vehicle exhibits unstable over-steer, excessive side-slip angles, and yaw rates. The saturation balancing control does provide stability as expected. The handling response of the vehicle with the combined control (saturation balancing and direct yaw-moment control) shows improvements both in the stability and responsiveness as compared to the uncontrolled response.

To see the internal workings of the saturation balancing control during the maneuver, Figure 6 depicts the level of the front torque bias during the maneuver.

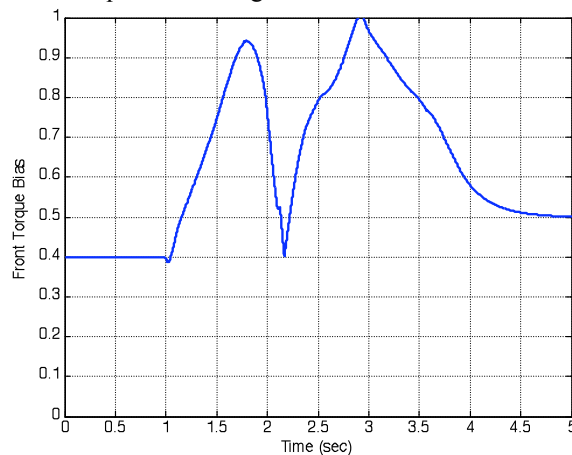


Fig. 6. Front Wheel Torque Bias (λ) for Combined Control

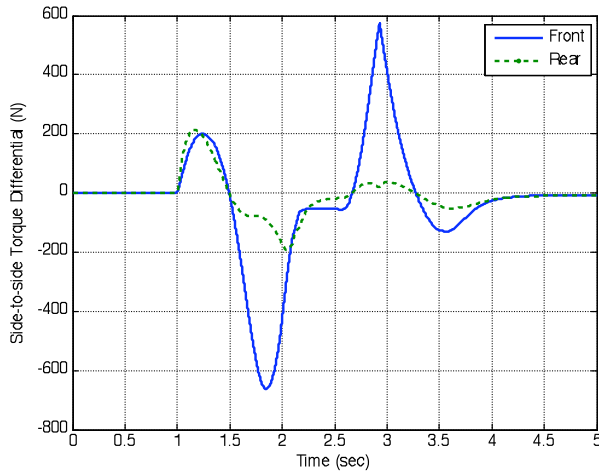


Fig. 7. Right-to-Left Torque Differential for Combined Control

The direct yaw-moment control is initially dominant in the maneuver due to insufficient yaw response, which can be seen by the side-to-side torque differentiation at time 1-2 seconds (Figure 7). However, the saturation balancing control becomes dominant later in the maneuver to counter impending over-steer seen in the uncontrolled response at time 2-4 seconds (Figure 6).

V. CONCLUSIONS

This paper discussed a new stability control strategy for a vehicle with an independent-wheel-drive architecture. Axle saturation is explicitly quantified and used in a feedback structure. This was then used along with a direct yaw-moment control component. The method enabled stabilization of a nominally over-steering vehicle while retaining yaw responsiveness. Simulation results revealed the benefits of each piece of the control scheme: the stable completion of the extreme avoidance maneuver due to the saturation balancing control as well as an improved response from direct yaw-moment control.

Further work on this topic will include using other feedback control schemes for vehicle stability control based on on-line estimated and explicitly quantified axle saturation levels. This includes predictive/optimal schemes that may improve the performance even more.

VI. NOMENCLATURE

A = vehicle frontal area
 A_y = lateral acceleration
 α_i = lateral slip angle of tire i
 C_D = drag coefficient
 C_{satF}, C_{satR} = Front/Rear Axle Saturation
 C_α = Cornering Stiffness
 F_x = longitudinal tire force
 F_y = lateral tire force
 F_z = normal tire load
 g = gravitational constant
 h_{cg} = vehicle C.G. height

h_{rcF}, h_{rcR} = front/rear roll center height
 I_{zz} = yaw inertia
 I_w = inertia of motor/wheel referred to wheel
 $K_{\phi R}, K_{\phi F}$ = rear/front roll stiffness
 K_{us} = Under steer Gradient
 K_p, K_b, K_D = Control Gains
 L = wheel base
 a, b = distance of front/rear axle from vehicle C.G.
 m = total vehicle mass
 R_w = effective wheel radius
 T_w = wheel torque
 d_f, d_r = front/rear wheel track width
 V_x = longitudinal velocity in vehicle x-axis
 V_y = lateral velocity in vehicle y-axis
 ω_i , or, ω_w = rotational speed of wheel i
 δ = road wheel steering angle
 ρ = density of air
 κ_i = longitudinal slip of tire i
 $\dot{\psi}$ = vehicle yaw rate
 λ = Front torque bias control variable

REFERENCES

- [1] Ghoneim, Y., et al., *Integrated Chassis Control System to Enhance Vehicle Stability*. International Journal of Vehicle Design, 2000. **Vol. 23**: p. 124-144.
- [2] Limroth, J., *Real-time Vehicle Parameter Estimation and Adaptive Stability Control*, in *Automotive Engineering*. 2009, Clemson University: Clemson, SC.
- [3] Rajamani, R., *Vehicle Dynamics and Control*. 2006.
- [4] Zanten, T.V., *Bosch ESP Systems: 5 Years of Experience*, in *SAE Automotive Dynamics & Stability Conference, SAE paper number 2000-01-1633*. 2000: Troy, MI.
- [5] Esmailzadeh, E., A. Goodarzi, and G.R. Vossoughi, *Directional stability and control of four-wheel independent drive electric vehicles*. Proc Instn Mech Engrs Part K: J Multi-body Dynamics, 2002. **216**(4): p. 303-313.
- [6] Goodarzi, A. and E. Esmailzadeh, *Design of a VDC System for All-Wheel Independent Drive Vehicles*. IEEE/ASME Transactions on Mechatronics, 2007. **12**(6): p. 632-639.
- [7] Karogal, I. and B. Ayalew, *Independent Torque Distribution Strategies for Vehicle Stability Control*. SAE paper number 2009-01-0456, 2009.
- [8] Osborn, R.P. and T. Shim, *Independent Control of All-Wheel-Drive Torque Distribution*. SAE paper number 2004-01-2052, 2004.
- [9] Piyabongkarn, D., et al., *On the Use of Torque-Biasing Systems for Electronic Stability Control: Limitations and Possibilities*. IEEE Transaction on Control Systems Technology, 2007. **15**(3): p. 581-589.
- [10] Gradu, M., *Torque Bias Coupling for AWD Applications*. SAE Paper No. 2003-01-0676, 2003.
- [11] Osborn, R. and T. Shim, *Independent Control of All-Wheel-Drive Torque Distribution*, in *SAE Automotive Dynamics, Stability & Controls Conference and Exhibition*. 2004: Detroit, MI.
- [12] Genta, G., *Motor Vehicle Dynamics: Modeling and Simulation*. Series on Advances in Mathematics for Applied Sciences. Vol. 43. 1997, Singapore: World Scientific
- [13] Pacejka, H.B., *Tyre and Vehicle Dynamics*. 2002, Oxford: Butterworth-Heinemann.
- [14] Fukada, Y., *Slip-Angle Estimation for Vehicle Stability Control*. Vehicle System Dynamics: International Journal of Vehicle Mechanics and Mobility, 1999. **Vol. 32**(No. 4): p. 375 - 388.
- [15] Osborn, R.P. and T. Shim, *Independent Control of All-Wheel-Drive Torque Distribution*. SAE paper number 2004-01-2052, 2004.

- [16] Karogal, I. and B. Ayalew, *Independent Torque Distribution Strategies for Vehicle Stability Control*, in *World Congress of the Society of Automotive Engineers*. 2009, SAE, Inc.: Detroit, MI.
- [17] NHTSA, *FMVSS 126- Electronic Stability Control Systems; Controls and Displays; 49 CFR Parts 571 and 585*, U.D.o.T. National Highway Traffic Safety Administration (NHTSA), Editor. 2007.